Measurements and analysis of helium-like triplet ratios in the X-ray spectra of O-type stars

Maurice A. Leutenegger and Frits B. S. Paerels

Department of Physics and Columbia Astrophysics Laboratory

Columbia University, 550 West 120th Street, New York, NY 10027, USA

maurice@astro.columbia.edu

Steven M. Kahn

Kavli Institute for Particle Astrophysics and Cosmology, Stanford Linear Accelerator and Stanford University

2575 Sand Hill Road, Menlo Park, CA 94025

David H. Cohen

Department of Physics and Astronomy

Swarthmore College, 500 College Avenue, Swarthmore, PA 19081

Received ____________________; accepted ____________________

ABSTRACT

We discuss methods of measuring and interpreting the forbidden to intercombination line ratios of helium-like triplets in the X-ray emission of O-type stars. Measurements are made for four O stars using archival *Chandra* data. We find minimum radii of formation typically in the range of $1.25 < r_{\rm min}/R_* < 1.67$, which is consistent with results obtained from line profile fits. However, these radii are generally inside the radii of optical depth one calculated from the measured mass loss rates. We find no evidence for anomalously low f/i ratios that require magnetically confined coronae or X-ray emitting plasmas at radii that are too small to generate X-ray emitting shocked plasma, as suggested in Waldron & Cassinelli (2001) and Cassinelli et al. (2001).

1. Introduction

Since the discovery of X-ray emission from OB stars by *Einstein* (Harnden et al. 1979; Seward et al. 1979), the exact mechanism for X-ray production has been something of a mystery. Although some models invoking magnetically confined coronae were put forward (Cassinelli & Olson 1979; Waldron 1984), these were not favored by the available spectral data, which showed substantial X-ray emission at low energies, which would not have been observable in a base corona because of photoelectric absorption in the dense stellar wind (Cassinelli & Swank 1983).[1] Also, a coronal model is not favored because the coronal mechanism is not thought to operate in hot stars, because outside of the core heat is

[1](This may be a less valid criticism in light of recent observations suggesting clumped winds and lower mass loss rates (Crowther et al. 2002; Massa et al. 2003; Hillier et al. 2003; Bouret, Lanz, & Hillier 2005).)

transferred radiatively and not by convection. Shocks arising from instabilities in the stars' radiatively driven winds are generally considered to be the most likely origin for X-ray emission (Lucy & White 1980; Lucy 1982; Owocki, Castor & Rybycki 1988; Feldmeier 1995). However, there have been difficulties in reproducing the observed X-ray properties of O-stars, such as the overall X-ray luminosity and the spectral energy distribution, from stellar wind instability models. Until recently, the quality of the available spectral data provided little insight into these problems, since the CCD and proportional counter spectra could not resolve individual lines.

Recent high resolution X-ray spectroscopy of OB stars by the *XMM-Newton* Reflection Grating Spectrometer (RGS) (Kahn et al. 2001) and the *Chandra* High Energy Transmission Grating Spectrometer (HETGS) (Schulz et al. 2000; Waldron & Cassinelli 2001; Cassinelli et al. 2001; Miller et al. 2002; Cohen et al. 2003) have answered some questions while raising new ones. Some stars have X-ray spectra that appear somewhat consistent with the idea that the X-rays are emitted in the wind, but there have been difficulties reconciling the data with specific models, leading to the resurrection of the idea that coronal mechanisms could be responsible for some of the X-ray emission in ζ Ori (Waldron & Cassinelli 2001). In their study of the HETGS spectrum of ζ Pup, Cassinelli et al. (2001) find that some of the X-ray emitting plasma may be emitted much closer to the stellar surface than one would expect, given the velocity law of the wind (within 0.2 stellar radii). Other stars (θ^1 Ori C and τ Sco) have X-ray spectra that seem to require models of X-ray emission that are quite different from the canonical stellar wind picture, even if a wind is still important in the model (Schulz et al. 2000; Cohen et al. 2003; Schulz et al. 2003; Gagne et al. 2005). Finally, for all of the O giants and supergiants observed, the profile asymmetries are less than one might expect, given the high mass loss rates measured for these stars using radio free-free emission, H α emission, and UV absorption lines.

One of the key diagnostic measurements available to us in understanding the nature of X-ray emission in OB stars is the forbidden to intercombination line ratio in the emission from ions that are isoelectronic with helium. This ratio is sensitive to the UV flux, and thus to the proximity to the stellar surface. This allows us to constrain the location of the X-ray emitting plasma independently of other spectral data.

In this paper we will discuss methods for using the f/i ratio to constrain the location of X-ray emitting plasma in O-star stellar winds. In particular, we will discuss the effects of photospheric absorption lines, as well as the f/i ratio expected for a plasma emitted over a range of radii.

These methods will then be applied to He-like triplet emission in a set of archival *Chandra* observations of O-stars. It will be shown that we find substantial disagreement with some previous measurements, even regardless of any difference in method of analysis or interpretation.

This paper is organized as follows: In § 2 we will review the physics of line formation in He-like species and discuss simple models useful for analyzing He-like triplet ratios in OB stars. In § 3 we will discuss the reduction and analysis of archival O-star X-ray spectra with these models. In § 4 we will discuss the results of this analysis. In § 5 we will give our conclusions.

2. Model

2.1. Radial dependence of the f/i ratio

The physics of helium-like ions in coronal plasmas has been investigated in numerous papers (Gabriel & Jordan 1969; Blumenthal, Drake, & Tucker 1972; Gabriel & Jordan 1973; Mewe & Schrijver 1975, 1978a,b,c; Pradhan & Shull 1981; Pradhan 1982; Porquet et al. 2001). The principal diagnostic is the ratio of the strengths of the forbidden to intercombination lines, $R \equiv f/i$.

The upper level of the forbidden line ($2\,^3S_0$) is metastable and relatively long-lived. When the excitation rate from $2\,^3S_0$ to the upper level of the intercombination line ($2\,^3P_{1,2}$) becomes comparable to the decay rate of the forbidden transition, the line ratio is altered. The excitations may be due to electron impacts in a high density plasma, or due to an external UV radiation source.

Gabriel & Jordan (1969) (hereafter GJ) and Blumenthal, Drake, & Tucker (1972) (BDT) derive the expression

$$R = R_0 \frac{1}{1 + \phi/\phi_{\rm c} + n_{\rm e}/n_{\rm c}}$$

ϕ is the photoexcitation rate from $2\,^3S$ to $2\,^3P$, and $\phi_{\rm c}$ is the critical rate at which R is reduced to $R_0/2$. Similarly, $n_{\rm e}$ is the electron density, and $n_{\rm c}$ is the critical density. The values of the critical flux and critical density have been calculated in BDT, as well as in other works. We adopt the BDT values here because they have calculated $\phi_{\rm c}$ for all the ions we are interested in, and because more recent calculations are not substantially different.

Because densities high enough to cause a change in the line ratios exist only very close to the star, we will consider only the photoexcitation term. The question of whether high densities are necessary to explain any of the observed ratios will be addressed in the discussion.

The expression for ϕ may be evaluated as follows, given a model stellar atmosphere flux H_ν:

$$\phi = B_{\rm lu}\, J_\nu = \frac{16\pi^2 e^2}{m_{\rm e} c}\, f\, \frac{H_\nu}{h\nu}\, W(r)$$

The expression derived by GJ is written such that f is the sum of the oscillator strengths for $2\,^3S_1$ to all three of $2\,^3P_J$, despite the fact that $2\,^3P_0$ does not decay to ground, and $2\,^3P_2$ only contributes for high Z. For low Z (Ne IX and lower) H_ν should be evaluated for $2\,^3S_1 \rightarrow 2\,^3P_1$. For Mg XI and higher Z ions it is more accurate to evaluate H_ν for both $2\,^3S_1 \rightarrow 2\,^3P_1$ and $2\,^3P_2$ and weight the average by the relative contributions to the effective branching ratio. Of course, this is only necessary if H_ν is substantially different for the two transitions.

Since the flux of UV radiation seen by ions in a stellar wind decreases in proportion to the geometrical dilution factor $W(r) = \frac{1}{2}(1 - \sqrt{1 - (R_*/r)^2})$, the value of R will also be a function of radius. It is helpful to express $R(r)$ in this form:

$$R(r) = R_0 \, \frac{1}{1 + 2\,P\,W(r)}$$

with $P = \phi_*/\phi_{\rm c}$ and

$$\phi_* = 8\pi \, \frac{\pi e^2}{m_{\rm e} c} \, f \, \frac{H_\nu}{h\nu}$$

2.2. The effect of photospheric absorption lines

The expression for $R(r)$ written in the last paragraph involves an approximation that must be explored further. We assumed a photospheric UV flux that would be diluted by geometry, but we neglected the Doppler shift of the absorbing ions. Over the range of Doppler shifts seen in a stellar wind, there can be many photospheric absorption lines. This introduces an additional radial dependence to the line ratio:

$$J_\nu = 4 H_{\nu({\rm r})} W(r)$$

with the Doppler shifted frequency as seen by an ion at radius r:

$$\nu(r) = \nu_0 \left(1 + \frac{v(r)}{c}\right)$$

In this expression, we do not adhere to the convention that a positive velocity results in a redshift.

In Figure 1 we show a plot of the photospheric UV flux for a model representing ζ Ori near the $2\,^3S_1 \rightarrow 2\,^3P_{1,2}$ transitions of Mg XI. The model is taken from the TLUSTY O-star model grid (Lanz & Hubeny 2003). Note that for Mg XI, most of the intercombination line strength still arises from the $2\,^3P_1$ to ground transition.

In order to assess the importance of explicitly accounting for photospheric lines in the R ratio, we will also compute R using an average value of H_ν. When the photoexcitation rate is not comparable to the critical rate the effect of photospheric lines on R is small. Therefore, we take the average value of H_ν over the range where $0.1 < R/R_0 < 0.9$. This range is estimated using the continuum UV flux. In cases where R does not go to 0.1, we average from zero velocity to the velocity at which $R = 0.9$.

In Figure 2 the dashed lines show R(r) for averaged and non-averaged H_ν for Mg XI for the star ζ Ori. There are substantial fluctuations in R(r) for the non-averaged case. The solid lines in the figure are discussed in the following section.

In making this figure we have ignored all additional Doppler shifts, as the purpose of the plot is mainly to illustrate qualitatively the effect of photospheric absorption lines on the R ratio. Examples of potentially relevant Doppler shifts are the thermal velocities of the ions (of order $100\,\mathrm{km\,s^{-1}}$ for Neon at 0.4 keV), stellar rotation (typically $100 - 200\,\mathrm{km\,s^{-1}}$ for O-type stars, although the wind also rotates), and the non-monotonicity of the stellar wind due to shocks (e.g. Feldmeier (1995), of order a few $100\,\mathrm{km\,s^{-1}}$). We have also treated the star as a point source rather than a finite disk, which would change the projected velocity as a function of position on the stellar disk.

2.3. The integrated ratio

In the preceding sections we calculated the radial dependence of the f/i ratio. However, we cannot directly observe the ratio as a function of radius, but only the overall ratio, or the ratio as a function of the observed Doppler shift. For any realistic model of a stellar wind, we expect the X-ray emitting plasma to be distributed over a large range of radii (although it could be a small range of radii for a coronal model). We can make an estimate for the ratio expected in a simplified version of the Owocki & Cohen (2001) (hereafter OC) model. This model is discussed in more detail in the next section, and in much greater detail in the original work. If the radial filling factor $f(u)$ is a constant and we neglect photoelectric absorption, the integrated ratio will be

$$R_{\rm int}(u_{\rm max}) = \frac{\int_0^{u_{\rm max}} \frac{du}{w^3(u)} f(u)}{\int_0^{u_{\rm max}} \frac{du}{w^3(u)} i(u)}$$

where $f(u) = G\frac{R(u)}{1+R(u)}$ and $i(u) = G\frac{1}{1+R(u)}$. In these expressions, $u = R_*/r$ is the inverse radial coordinate, and $w(u) = v(u)/v_\infty$ is the scaled velocity. G is the ratio $(f+i)/r$, and $R(u)$ was derived in the previous sections. $u_{\rm max}$ is the inverse of the minimum radial cutoff for X-ray emission, $R_{\rm min}$. Considering the results of Kramer et al. (2003), neglecting absorption and taking the radial filling factor to be a constant are not unreasonable approximations, at least to gain an understanding of the characteristic behavior of the R ratio as a function of u or u_{max}.

In Figure 2, the solid lines show the integrated f/i ratio as a function of $u_{\rm max}$ for Mg XI in ζ Ori. The integrated ratio is very similar for both the averaged flux and unaveraged flux cases. Since it much simpler to consider only a single value of photospheric UV flux, we will do so in the rest of this paper. However, it should be noted that if one modelled the X-ray emission as arising near a single radius or doppler shift, the actual photospheric flux (including absorption lines) would have to be included in the modeling.

Also, regardless of photospheric absorption lines, there are relatively large uncertainties in the EUV continuum flux shortward of the Lyman edge, which has never been directly observed in an O-star. This will affect predictions for Si XIII and higher Z elements.

In Figures 3,4,5, and 6, we show $R(u)$ and $R_{\rm int}(u_{\rm max})$ for all ions observed in four O stars. For a given measured value of R, there are substantial differences between the value of $u_{\rm max}$ derived assuming a distributed plasma and the value of u derived assuming a plasma dominated by one radius - that is, $u_{\rm max}$ will always be larger than u for a single radius.

2.4. He-like line profiles

Although it may sometimes be easier to measure the f/i ratio directly and compare it to a calculation for the ratio as a function of distance from the star, it is potentially much more powerful to calculate line profiles including the radial dependence of the line ratio and compare these to the data. The expression for the line profile derived in Owocki & Cohen (2001) is

$$L_{\rm x} = C \int_0^{u_{\rm x}} du \frac{f_{\rm r}(u)}{w^3(u)} e^{-\tau}$$

In this expression, the radial filling factor is $f_{\rm r}(u) = u^{\rm q}$.

To account for the relative line strengths of the triplet, we simply multiply the integrand with $f(u) = G\frac{R(u)}{1+R(u)}$ or $i(u) = G\frac{1}{1+R(u)}$. This normalizes the forbidden and intercombination lines to the resonance line, which may be calculated using the above expression with no modification.

In comparison with the integrated plots presented in the previous section, a line profile with $\tau_* > 0$ will have a higher R ratio than one with no absorption, given the same value of $u_{\rm max}$. This is because the forbidden line will only be formed further out where absorption is less, while the intercombination line is mainly formed close to the star, where absorption is greater. Nonzero positive values of q will cause R to go down, because relatively more emission will come from close to the star, while negative values will cause R to go up.

In the next section, we will use this model to fit Chandra HETGS spectra of four O stars.

3. Data reduction and analysis

In this section we will fit He-like triplets in the *Chandra* HETG data of four O-stars: ζ Pup, ζ Ori, ι Ori, δ Ori. We will measure the ratios only for Mg XI, Si XIII, and for ζ Pup S XV. Ne IX and lower Z He-like species generally have $R < 0.2$ in O-stars and therefore do not contain much information in the line ratio, although the profiles may be jointly fit to get the same information one would obtain from a Ly α line.

3.1. Data processing

Primary data products were obtained from the *Chandra* data archive and processed using standard CIAO routines outlined in the CIAO user manual in the grating spectroscopy threads. The versions used were CIAO 3.1 and CALDB 2.28. The spectral fitting was done with XSPEC 11.3.1. The C statistic is used instead of χ^2 because of the low number of counts per bin. All fitting was done with MEG ± 1 orders, which were not coadded, but were fit simultaneously. For ζ Ori and ι Ori the data were split into two observations each, which were fit simultaneously. Emission lines were fit over a wavelength range of

$(\lambda_{\rm r}(1 - v_\infty/c) - \Delta\lambda,\ \lambda_{\rm f}(1 + v_\infty/c) + \Delta\lambda)$, where $\Delta\lambda$ is the resolution of MEG at that wavelength.

3.2. Fitting procedure

We use two different fitting procedures, depending on the number of counts in the triplet. For triplets with many counts (Mg XI for all stars, and Si XIII for ζ Pup), we fit them with the He-like OC profile described in Section 2.4. The fixed model parameters are the line rest wavelengths, the terminal velocity of the wind, the velocity law $\beta = 1$, R_0, and the photospheric UV strength. The fit parameters from the profile model are q, τ_*, and $u_{\rm max}$, in addition to the G ratio and the overall normalization. The four fit parameters other than normalization are fit on a grid with spacing 0.2 for q and τ_*, and spacing 0.05 for $u_{\rm max}$ and G.

For lines with few counts (S XV for ζ Pup and Si XIII for the other stars), we fit them with a three Gaussian model. This is because it is best to use a simpler model when the number of counts is small enough to prevent a more complex model from fitting the data significantly better. Rather than using three individual gaussians, which would have three separate normalizations, we use a model with parameters G, R, the overall normalization, and the velocity width, which is taken to be the same for all the lines in a given complex.

In both cases we add a continuum component to approximate bremsstrahlung emission. This is represented by a power law of index 2 with normalization chosen to fit the continuum near the line. Care is taken to avoid including moderately weak spectral lines in the continuum fit. A power law of index 2 is not necessarily appropriate for the continuum in general, but over a sufficiently short range in wavelength, any reasonable continuum is statistically indistinguishable. An index of 2 is chosen because this gives a flat continuum when plotted versus wavelength.

We do not expect any other strong lines to contaminate our line fits. Mg XII Ly γ is at approximately the same wavelength as the Si XIII forbidden line, but even in ζ Ori, where Si XIII is relatively weak, the strength of Mg XII Ly γ expected given the strength of Ly α is not enough to affect our measurements significantly.

3.3. Results

The results of the fits are summarized in Tables 3 and 4. The fits are plotted with the data in Figures 7, 8, 9, 10, 11, 12, 13, 14, 15, 16, and 17. Two parameter confidence interval plots for the profile fits are given in Figures 18, 19, 20, 21, and 22.

The goodness of fit is tested by comparing the fit statistic to that obtained from Monte Carlo simulations from the model. The percentage of 1000 realizations having C less than the data is given in the tables of results.

The helium-like line profile fits generally are adequate to explain the data, although the fits to Mg XI in ζ Ori and ι Ori and Si XIII in ζ Pup are marginal (each has approximately 80% of MC realizations of the model with C less than that of the data). The fact the the fits can simultaneously account for the profile shape and the f/i ratio indicates that the values of $u_{\rm max}$ obtained are not an artifact of the profile model.

The fit parameters obtained are generally consistent with those obtained in Kramer et al. (2003) and Cohen et al. (2006). The R ratios for the helium-like line profile fits are also consistent with those measured in Kahn et al. (2001),Waldron & Cassinelli (2001), and Cassinelli et al. (2001). The values of $u_{\rm max}$ for all four stars fall in the range $0.6 < u_{\rm max} < 0.8$, or $1.25 < R_{\rm min} < 1.67$. This is substantially closer to the star than inferred in Kahn et al. (2001), Waldron & Cassinelli (2001), and Cassinelli et al. (2001), mainly because these papers assumed a single radius of formation.

None of the low-statistics lines strongly constrains the R ratio, and all of them are consistent with $R = R_0$. The goodness of fit is acceptable, except for ζ Ori. However, in the case of the Si XIII complex of ζ Ori, the positive and negative first order data are very different, and it is possible to get a satisfactory fit by fitting only the positive first order. It is not clear why the positive and negative first orders should be so different, or whether this represents only a random statistical fluctuation or a real calibration issue.

The results for the R ratios of Si XIII in ζ Ori and S XV in ζ Pup contradict the measurements of Waldron & Cassinelli (2001) and Cassinelli et al. (2001). It is not clear why this is, as the exact methodology used to obtain the measurements is not reported by those authors. One possibility is that the χ^2 statistic was used, even though it is not valid for the non-Poisson regime. Another possibility is that the fitting algorithm used had difficulty due to correlation in the measurement of the normalization of the forbidden and intercombination lines, causing it to get stuck in a local minimum. This is a problem that we have avoided by using G and R as model parameters instead, so that any insensitivity of the model parameter to the data is captured explicitly in the error on that parameter. Another possibility is that the three gaussians used to fit the data were allowed to have three independent widths, which could lead to strange results if one of the gaussians was much wider.

The values of $u_{\max}$ allowed by the R values measured in the low-statistics lines are generally consistent with those obtained by profile-fitting to the high-statistics lines, for a given star.

4. Discussion

We have used the f/i ratios of He-like triplets in conjunction with their line profiles to constrain the radial distribution of X-ray emitting plasma in O-stars. Our results are consistent with the results of Kramer et al. (2003) and Cohen et al. (2006), in the sense that the values of $u_{\max}$ are similar. We also find that the optical depths are constrained to be smaller than one would expect, given the published mass loss rates, although these lines give poorer constraints on the optical depth - mass loss rate discrepancy than longer wavelength lines, where the photoelectric absorption cross-section per unit mass is higher.

Our results for S XV in ζ Pup and Si XIII in ζ Ori are inconsistent with those of Waldron & Cassinelli (2001) and Cassinelli et al. (2001). For S XV in ζ Pup we measure $R = 1.0^{+1.4}_{-0.6}$, while Cassinelli et al. (2001) measure $R = 0.61 \pm 0.48$. For Si XIII in ζ Ori we measure $R \geq 2.4$, while Waldron & Cassinelli (2001) measure $R = 1.2 \pm 0.5$.

This calls into question the claim that the f/i ratio in these stars indicates some sort of anomalous behavior. In Waldron & Cassinelli (2001) it is suggested that high plasma densities close to the star could explain the f/i ratio, which their measurements indicate may be too low for the photospheric UV excitation effect to achieve. Even if photospheric UV excitation is sufficient to explain the observed ratio, it would only be sufficient very close to the star ($< 1.1\,R_*$), and the authors hypothesize that this could indicate the existence of a magnetically confined corona, as this would be too close to the star for strong shocks to develop. In Cassinelli et al. (2001) the radius of formation for S XV is also claimed to be too small ($< 1.2\,R_*$) to allow shocks of the required velocity to develop. Note that our claim of a larger radius of formation for S XV in ζ Pup and S XIII in ζ Ori is based entirely on our different measurements of the R ratio, and not due to a difference in the methodology of inferring a radius from the R ratio. In fact, for a given R ratio, assuming a distribution of radii gives a value of $R_{\min}$ that is smaller than the radius one would obtain assuming the plasma to originate at only one radius.

It should also be pointed out that, regardless of the actual measurements of the R ratio, the exciting wavelengths for Si XIII and S XV lie on the short wavelength side of the Lyman break. There are no measurements of the photospheric UV flux at these wavelengths for any O-stars, and the model fluxes are substantially more uncertain. Furthermore, the effective temperature scale used for O-stars in the past may be systematically too high (Martins, Schaerer, & Hillier 2002), which would also have more of an effect on the part of the spectrum shortward of the Lyman break. The change in the effective temperature scale would make the photospheric UV flux shortward of the Lyman break smaller, thus making it more difficult to explain an altered R ratio in Si XIII or S XV using UV photoexcitation, if an altered ratio were observed.

Figure 2 of Cassinelli et al. (2001) compares the radii they infer from measurements of f/i ratios in He-like triplets in ζ Pup to the radius of optical depth one, R_1, for the wavelength at which that He-like ion emits. They claim that the inferred radii correspond roughly to R_1, so that we are observing plasma at the closest point to the star where we can see it. Kahn et al. (2001) make a similar conjecture. Table 5 compares the values of R_1 from Cassinelli et al. (2001) to those derived using the methodology of this paper. For both Ne IX and Mg XI the measured values of $R_{\rm min}$ place the X-ray emitting plasma far inside the calculated radius of optical depth one. In light of the measurements of Kramer et al. (2003) and Cohen et al. (2006), this is not surprising, since the optical depths inferred from profile fitting are much lower than those predicted from the literature mass loss rates.

5. Conclusions

We have investigated the effect of a radially distributed plasma on the forbidden to intercombination line ratio in helium-like triplets, as well as variations in the exciting photospheric flux as a function of Doppler shift throughout the wind. We find that the fact that the plasma is likely distributed over a range of radii and Doppler shifts allows us to use an averaged value of the photospheric continuum instead of accounting for it in detail. We also find that the value of u_{max} derived assuming a distribution of radii is substantially smaller than the value of u derived assuming a single radius.

We have used the f/i ratio of helium-like triplets to constrain the radial distribution of X-ray emitting plasma in four O-type stars. We find that the minimum radius of emission is typically $0.6 < u_{\mathrm{max}} < 0.8$, or $1.25 < r_{\mathrm{min}}/R_* < 1.67$. This is consistent with the results of line profile fits using the model of Owocki & Cohen (2001) (Kramer et al. 2003; Cohen et al. 2006). However, these radii of formation are typically well inside the radius of optical depth unity calculated using the mass loss rates in the literature.

We find that there is no evidence for anomalously low f/i ratios in high-Z species, as claimed in Waldron & Cassinelli (2001) and Cassinelli et al. (2001). There is no need to invoke magnetically confined plasmas to explain the data, nor are the X-rays emitted from regions that are too close to the star to have an adequate shock jump. This conclusion is based solely on different measured values obtained from the data, and does not depend on any modelling assumptions.

We have fit He-like emission line complexes with profile models that simultaneously account for profile shapes and line ratios. These models constrain the radial distribution of plasma both through the line ratio and the profile parameters u_{max} and q. We find that they are capable of producing acceptable fits to the data, showing that the information contained in the line ratios and profile shapes are mutually consistent.

REFERENCES

Blumenthal, G. R., Drake, G. W. F., & Tucker, W. H. 1972 ApJ 172, 205

Bouret, J. C., Lanz, T., & Hillier, D. J. 2005 astro-ph 0412346

Cassinelli, J. C., & Olson, G. L. 1979 ApJ 229, 304

Cassinelli, J. C., & Swank, J. H. 1983 ApJ 271, 681

Cassinelli, J. C., Miller, N. A., Waldron, W. L., Macfarlane J. J., & Cohen D. H. 2001 ApJ 554, 55L

Cohen, D. H., de Messières, G. E., MacFarlane, J. J., Miller, N. A., Cassinelli, J. P., Owocki, S. P., & Liedahl, D. A. 2003 ApJ 586, 493

Cohen et al. 2006 In preparation

Crowther, P. A., Hillier, D. J., Evans, C. J., Fullerton, A. W., De Marco, O., & Willis, A. J. 2002 ApJ 579, 774

Dere, K. P., Landi, E., Mason, H. E., Mongsignori Fossi, B. C., & Young, P. R. 1997 A&AS 125, 149

Feldmeier, A. 1995 A&A 299, 823

Gabriel, A. H., & Jordan, C. 1969 MNRAS 145, 241

Gabriel, A. H., & Jordan, C. 1973 ApJ 186, 327

Gagne, M., Oksala, M. E., Cohen, D. H., Tonnesson, S. K., ud-Doula, A., Owocki, S. P., Townsend, R. H. D., Macfarlane, J. J. 2005 astro-ph/0504296

Harnden, F. R., Jr., Branduardi, G., Gorenstein, P., Grindlay, J., Rosner, R., Topka, K., Elvis, M., Pye, J. P., Vaiana, G. S. 1979 ApJ 234 51L

Hillier, D. J., Lanz, T., Heap, S. R., Hubeny, I., Smith, L. J., Evans, C. J., Lennon, D. J., & Bouret, J. C. 2003 ApJ 588, 1039

Kahn, S. M., Leutenegger, M. A., Cottam, J., Rauw, G., Vreux, J.-M., den Boggende, A. J. F., Mewe, R., Güdel, M. 2001 A&A 365, 312L

Kramer, R. H., Cohen, D. H., & Owocki, S. P. 2003 ApJ 592, 532

Krolik, J. H., & Raymond, J. C. 1985 ApJ 298, 660

Lanz, T., & Hubeny, I. 2003 ApJS 146, 417

Lamers, H. J. G. L. M., & Leitherer, C. 1993 ApJ 412, 771

Lucy, L. B., & White, R. L. 1979 ApJ 241, 300

Lucy, L. B. 1982 ApJ 258, 186

Martins, F., Schaerer, D., & Hillier, D. J. 2002 A&A 382, 999

Massa, D., Fullerton, A. W., Sonnerborn, G., & Hutchings, J. B. 2003 ApJ 586, 996

Mewe, R., & Schrijver, J. 1975 Ap&SS 38, 345

Mewe, R., & Schrijver, J. 1978 A&A 65, 99

Mewe, R., & Schrijver, J. 1978 A&A 65, 115

Mewe, R., & Schrijver, J. 1978 A&AS 33, 311

Miller, N. A., Cassinelli, J. P., Waldron, W. L., Macfarlane, J. J., & Cohen, D. H. 2002 ApJ 577, 951

Owocki, S. P., Castor, J. I. & Rybicki, G. B. 1988 ApJ 335, 914

Owocki, S. P., & Cohen, D. H. 2001 ApJ 559, 1108

Porquet, D., Mewe, R., Dubau, J., Raasen, A. J. J., & Kaastra, J. S. 2001 A&A 376, 1113

Pradhan, A. K., & Shull, J. M. 1981 ApJ 249, 821

Prinja, R. K., Barlow, M. J., & Howarth, I. D. 1990 ApJ 361, 607

Schulz, N. S., Canizares, C. R., Huenemoerder, D., Lee, J. C. 2000 ApJ 545, 135L

Schulz, N. S., Canizares, C. R., Huenemoerder, D., Tibbets, K. 2003 ApJ 595, 365

Seward, F. D., Forman, W. R., Giacconi, R., Griffiths, R. E., Harnden, F. R., Jr., Jones, C., Pye, J. P. 1979 ApJ 234, 55L

Pradhan, A. K. 1982 ApJ 263, 477

Waldron, W. L. ApJ 282, 256

Waldron, W. L., & Cassinelli, J. P. 2001 ApJ 548, 45L

Young, P. R., Del Zanna, G., Landi, E., Dere, K. P., Mason, H. E., & Landini, M. 2003 A&AS 144, 135

This manuscript was prepared with the AAS LaTeX macros v5.2.

Ion	f ($2\,^3S_1 \rightarrow 2\,^3P_J$)	ϕ_c (s^{-1})	R_0	$G(T_{max})$
S XV	0.0507	9.16e5	2.0	
Si XIII	0.0562	2.39e5	2.3	0.68
Mg XI	0.0647	4.86e4	2.7	0.71
Ne IX	0.0700	7.73e3	3.1	0.74
O VII	0.0975	7.32e2	3.7	0.90
N VI	0.1136	1.83e2	5.3	0.88

Table 1: Parameters adopted for He-like triplets. Oscillator strengths are from CHIANTI (Dere et al. 1997; Young et al. 2003). ϕ_c are from BDT. R_0 and $G(T_{max})$ are from Porquet et al. (2001), except S XV, which is taken from BDT.

Star	T_{eff} (kK)	$\log g$ ($cm\,s^{-2}$)	v_{inf} ($km\,s^{-1}$)
ζ Pup	42.5	3.75	2485
ζ Ori	30.0	3.25	1860
ι Ori	35.0	3.50	2195
δ Ori	32.5	3.25	1995

Table 2: Adopted stellar parameters. T_{eff} and $\log g$ are the closest approximations to the values used in Lamers & Leitherer (1993) that are on the TLUSTY O star grid. Terminal velocities are taken from Prinja, Barlow, & Howarth (1990).

Star	Ion	q	τ_*	$u_{\rm max}$	$R_{\rm min}$	G	R	Flux	C	Bins	MC
ζ Pup	Mg XI	$0.0^{+0.4}_{-0.2}$	$1.0^{+0.4}_{-0.4}$	$0.70^{+0.05}_{-0.05}$	1.43	$0.70^{+0.15}_{-0.10}$	0.41	$17.7^{+0.9}_{-0.9}$	135.3	136	39.1
	Si XIII	$0.0^{+0.6}_{-0.4}$	$0.6^{+0.4}_{-0.2}$	$0.70^{+0.05}_{-0.10}$	1.43	$1.05^{+0.15}_{-0.15}$	0.90	$11.9^{+0.7}_{-0.7}$	116.2	98	84.7
ζ Ori	Mg XI	$-0.4^{+1.0}_{-0.2}$	$0.2^{+0.2}_{-0.2}$	$0.6^{+0.10}_{-0.1*}$	1.67	$1.05^{+0.05*}_{-0.2}$	0.82	$6.5^{+0.5}_{-0.6}$	267.2	240	73.4
ι Ori	Mg XI	$-0.8^{+0.2}_{-0.0}$	$0.0^{+0.2}_{-0.0}$	$0.75^{+0.05}_{-0.10}$	1.33	$0.90^{+0.20*}_{-0.25}$	0.72	$3.5^{+0.5}_{-0.5}$	266.6	256	80.2
δ Ori	Mg XI	$-0.8^{+0.4}_{-0.0}$	$0.0^{+0.2}_{-0.0}$	$0.80^{+0.05}_{-0.10}$	1.25	$0.60^{+0.25}_{-0.10*}$	0.75	$4.0^{+0.5}_{-0.5}$	123.9	124	18.2

Table 3: Parameters for He-like profile fits. Errors are 2σ, or $\Delta C = 4$. Flux is given in units of $10^{-5}\,{\rm photons\,cm^{-2}\,s^{-1}}$. MC is the percentage of Monte Carlo realizations of the model having C less than the data does for that model. Asterisks indicate parameters that were still within 2σ at the edge of the fit range.

Star	Ion	$\sigma_{\rm v}/c$ (10^{-3})	R	G	Flux	C	Bins	MC
ζ Pup	S XV	$2.6^{+0.6}_{-0.4}$	$1.0^{+1.6}_{-0.4}$	$0.7^{+0.3}_{-0.2}$	$3.3^{+0.7}_{-0.6}$	89.7	98	50.6
ζ Ori	Si XIII	2.2 ± 0.2	≥ 2.4	1.2 ± 0.2	2.4 ± 0.3	151.1	118	98.1
ζ Ori $m = +1$	Si XIII	2.0 ± 0.2	≥ 2.8	0.9 ± 0.2	2.4 ± 0.4	57.6	59	35.3
ζ Ori $m = -1$	Si XIII	$3.0^{+0.8}_{-0.6}$	≥ 1.6	$2.0^{+1.0*}_{-0.6}$	$2.4^{+0.6}_{-0.5}$	85.6	59	98.8
ι Ori	Si XIII	3.2 ± 0.4	≥ 1.8	1.8 ± 0.4	1.6 ± 0.3	169.7	236	27.8
δ Ori	Si XIII	0.6 ± 0.4	≥ 1.4	0.8 ± 0.1	1.7 ± 0.3	116.8	118	46.3

Table 4: Parameters for He-like Gaussian fits. Errors are 1σ, or $\Delta C = 1$. Asterisks indicate parameters that were still within 1σ at the edge of the fit range. Flux is in units of $10^{-5}\,\mathrm{photons\,cm^{-2}\,s^{-1}}$. MC is the percentage of Monte Carlo realizations of the model having C less than the data does for that model.

Ion	R_1	u_1	u_{max}	R_{min}
Mg XI	2.5	0.4	0.70 ± 0.05	1.43 ± 0.10
Ne IX	5	0.2	> 0.4	< 2.5
O VII	4	0.25	> 0.25	< 4

Table 5: Comparison of radius of optical depth unity calculated by Cassinelli et al. (2001) for ζ Pup with measured values of R_{min}, the minimum onset radius for X-ray emission. R_{min} is measured using an He-like line profile fit for Mg XI, and upper limits for O VII and Ne IX are derived from upper limits to the f/i ratio of $R < 0.1$ and $R < 0.2$, respectively. The same quantities are also reported in inverse radial coordinates.

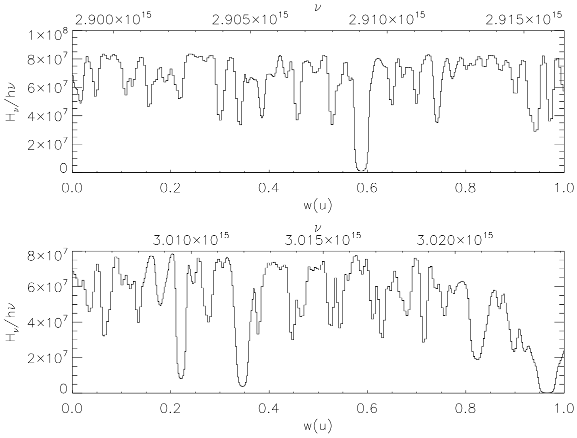

Fig. 1.— Model UV flux for ζ Ori near the $2\,^3S_1 \rightarrow 2\,^3P_{1,2}$ transitions of Mg XI ($J = 1$ is on the top, $J = 2$ on the bottom), plotted as a function of scaled stellar wind velocity, w (bottom axis), and frequency (top axis). The model flux is taken from the TLUSTY O-star grid (Lanz & Hubeny 2003).

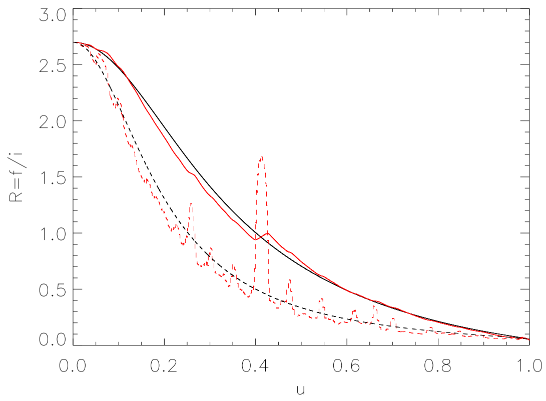

Fig. 2.— The f/i ratio for the Mg XI triplet of ζ Ori plotted as a function of the inverse radial coordinate $u = R_*/r$. The red lines are for the actual model photospheric UV flux, while the black lines are for an averaged value. The dashed lines denote the radial dependence of R and the solid lines show the R ratio observed for the whole star as a function of u_{max} (see text). The red lines include the effects of the photospheric UV flux for transitions to both the $2\,^3P_1$ and $2\,^3P_2$ states, although the $2\,^3P_1$ state is far more important. The peaks in the red dashed line correspond to the absorption lines in the top panel of Figure 1 plotted with the x-axis reversed. This is because $w = 1 - u$, and one figure is plotted against w, while the other is plotted against u.

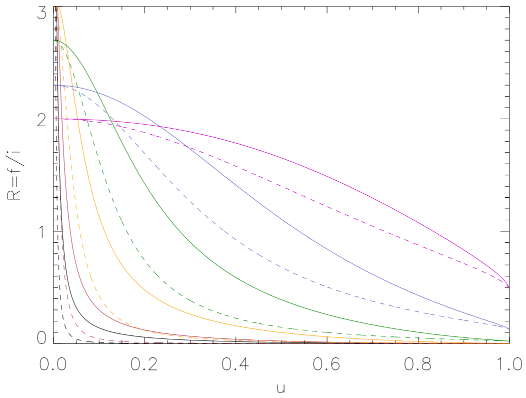

Fig. 3.— The f/i ratio for six He-like triplets observed in ζ Pup. The solid and dashed lines are as in Figure 2. Colors are black for N VI, red for O VII, orange for Ne IX, green for Mg XI, blue for Si XIII, and purple for S XV.

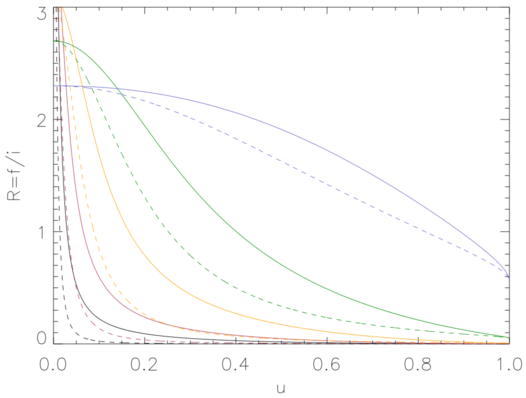

Fig. 4.— The f/i ratio for five He-like triplets observed in ζ Ori. Scheme is as in Figure 3.

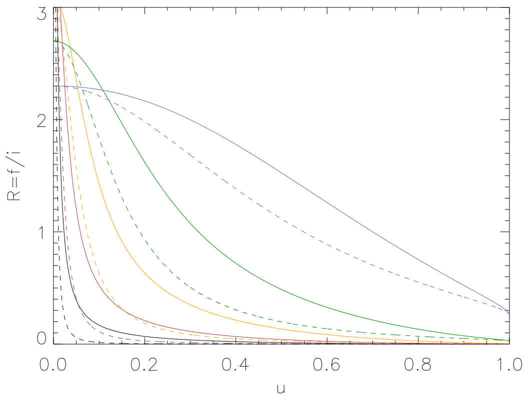

Fig. 5.— The f/i ratio for five He-like triplets observed in ι Ori. Scheme is as in Figure 3.

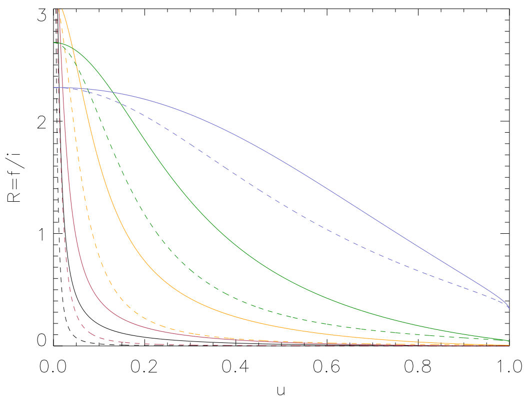

Fig. 6.— The f/i ratio for five He-like triplets observed in δ Ori. Scheme is as in Figure 3.

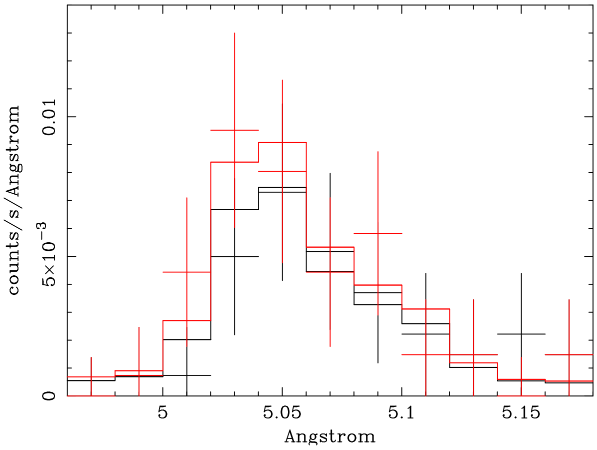

Fig. 7.— Data and best-fit model for S XV in ζ Pup. MEG -1 order is in white, MEG +1 is in red.

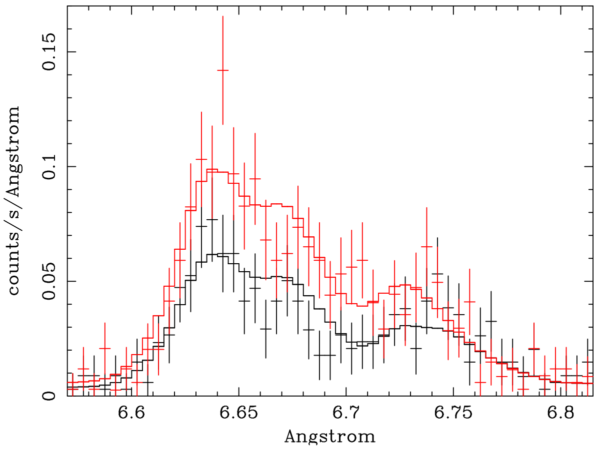

Fig. 8.— Data and best-fit model for Si XIII in ζ Pup.

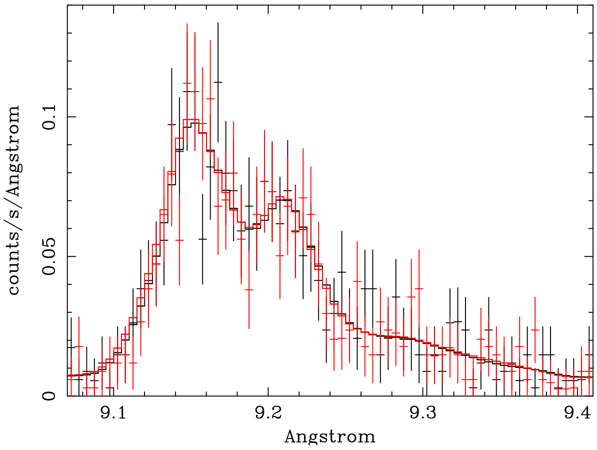

Fig. 9.— Data and best-fit model for Mg XI in ζ Pup.

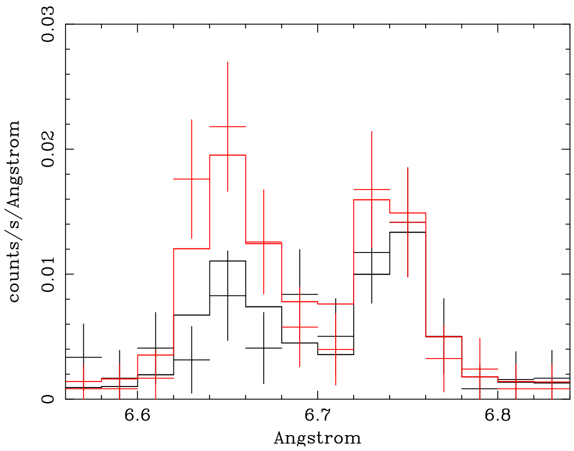

Fig. 10.— Data and best-fit model for Si XIII in ζ Ori.

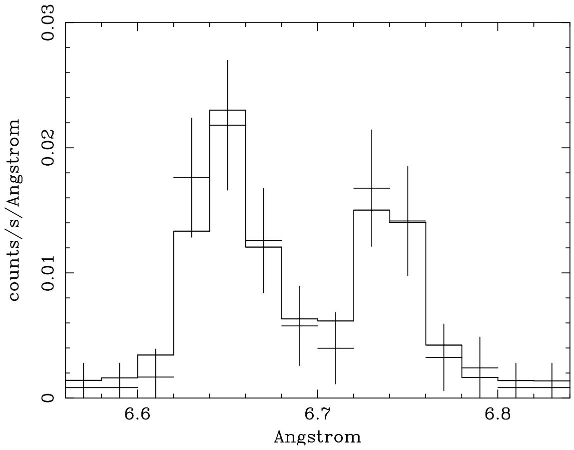

Fig. 11.— Data and best-fit model for Si XIII in ζ Ori, MEG +1 order.

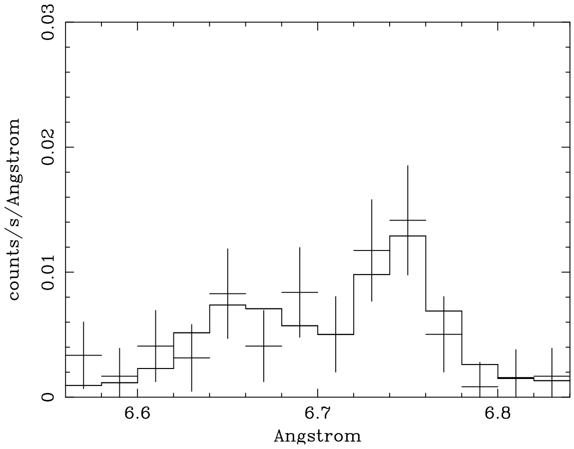

Fig. 12.— Data and best-fit model for Si XIII in ζ Ori, MEG -1 order.

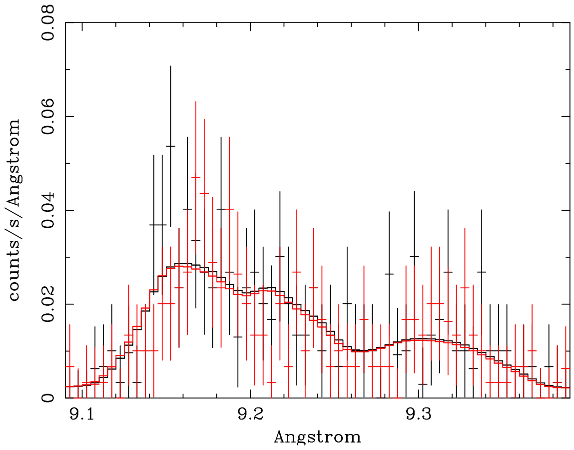

Fig. 13.— Data and best-fit model for Mg XI in ζ Ori.

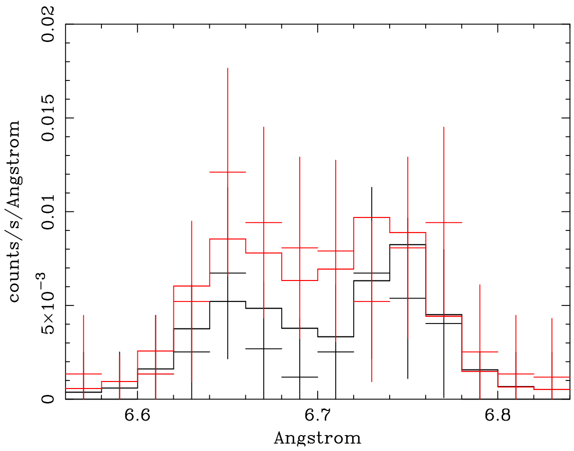

Fig. 14.— Data and best-fit model for Si XIII in ι Ori.

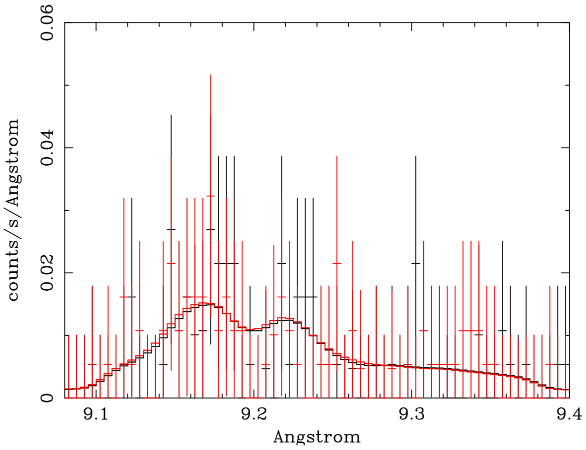

Fig. 15.— Data and best-fit model for Mg XI in ι Ori.

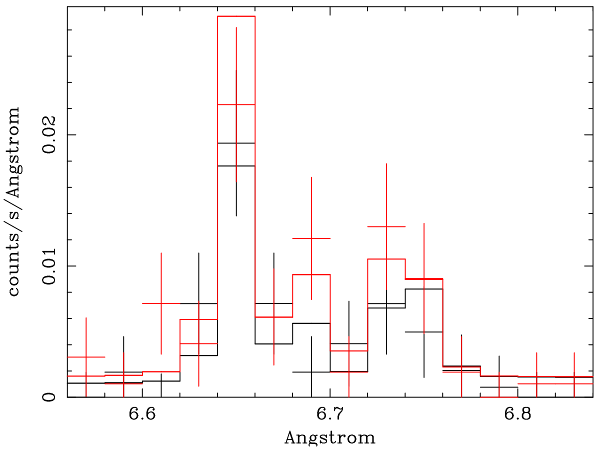

Fig. 16.— Data and best-fit model for Si XIII in δ Ori.

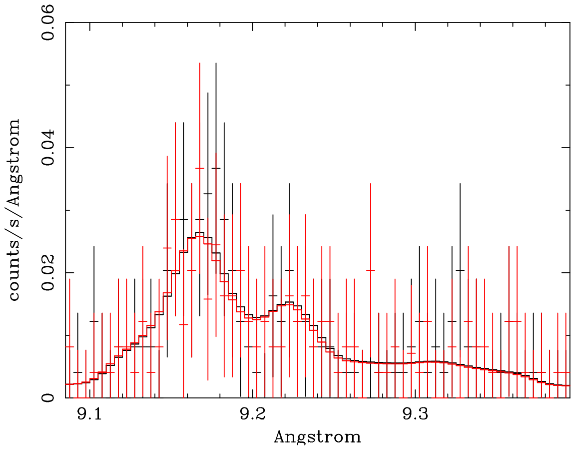

Fig. 17.— Data and best-fit model for Mg XI in δ Ori.

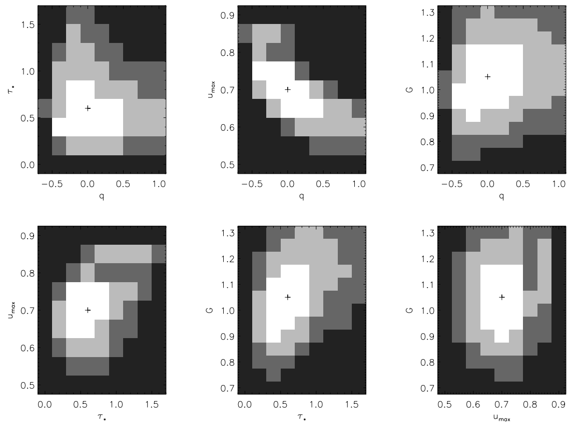

Fig. 18.— Two dimensional plots of confidence intervals for fit parameters for Si XIII in ζ Pup. The shades of grey represent 1, 2, and 3 σ, or $\Delta C < 2.3, 6.17, 11.8$.

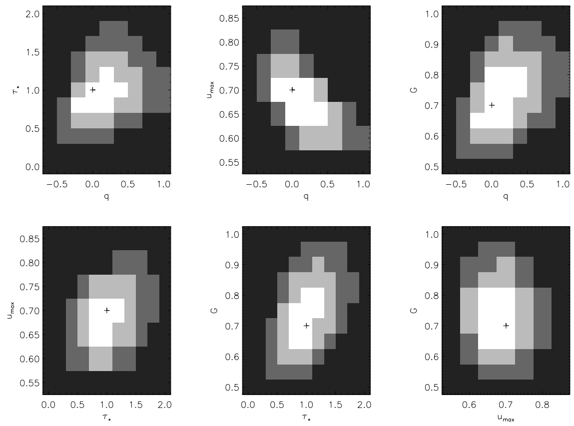

Fig. 19.— Same as Figure 18 for Mg XI in ζ Pup.

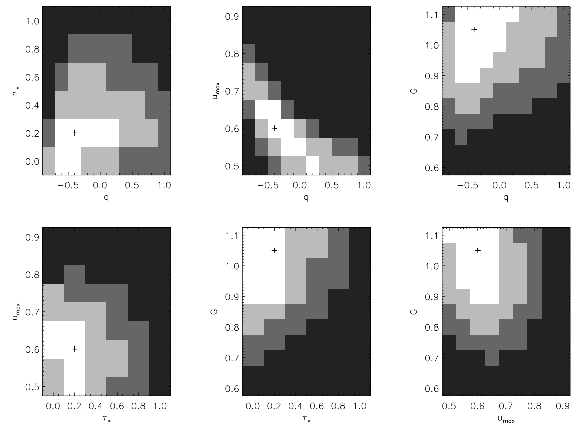

Fig. 20.— Same as Figure 18 for Mg XI in ζ Ori.

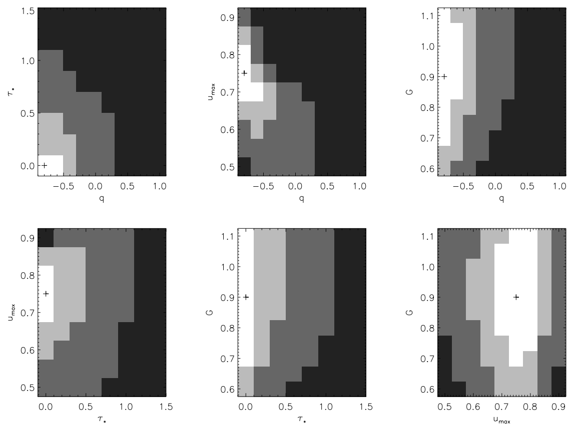

Fig. 21.— Same as Figure 18 for Mg XI in ι Ori.

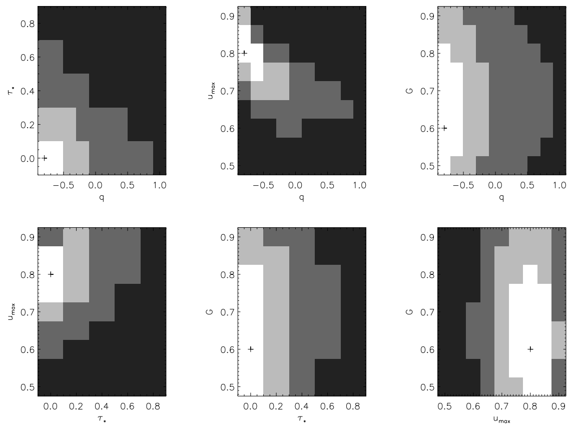

Fig. 22.— Same as Figure 18 for Mg XI in δ Ori.